Published in final edited form as:
Bioconjug Chem. 2010 December 15; 21(12): 2355–2360. doi:10.1021/bc100391a.

Radiofluorinated Rhenium Cyclized α-MSH Analogs for PET Imaging of Melanocortin Receptor 1

Gang Ren, PhD[1], **Shuanlong Liu, PhD**[1], **Hongguang Liu, PhD**[1], **Zheng Miao, PhD**[1], and **Zhen Cheng, PhD**[1,*]

[1]Molecular Imaging Program at Stanford (MIPS), Department of Radiology, and Bio-X Program, Canary Center at Stanford for Cancer Early Detection, Stanford University, Stanford, California, 94305-5344

Abstract

In order to accomplish *in vivo* molecular imaging of melanoma biomarker melanocortin 1 receptor (MC1R), several alpha-melanocyte-stimulating hormone (α-MSH) analogs have been labeled with *N*-succinimidyl-4-^{18}F-fluorobenzoate (^{18}F-SFB) and studied as positron emission tomography (PET) probes in our recent studies. To further pursue a radiofluorinated α-MSH peptide with high clinical translation potential, we utilized 4-nitrophenyl 2-^{18}F-fluoropropionate (^{18}F-NFP) to radiofluorinate the transition metal rhenium cyclized α-MSH metallopeptides for PET imaging of MC1R positive malignant melanoma.

Methods—Metallopeptides Ac-d,Lys-ReCCMSH(Arg^{11}) (two isomers, namely **RMSH-1** and **RMSH-2**) were synthesized using conventional solid phase peptide synthesis chemistry and rhenium cyclization reaction. The two isomers were then conjugated with ^{19}F-NFP or ^{18}F-NFP. The resulting cold or radiofluorinated metallopeptides, **$^{18/19}$F-FP-RMSH-1** and **$^{18/19}$F-FP-RMSH-2** were further evaluated for their *in vitro* receptor binding affinities, *in vivo* biodistribution and small-animal PET imaging properties.

Results—The binding affinities of the **^{19}F-FP-RMSH-1** and **^{19}F-FP-RMSH-2)** were determined to be within low nM range. *In vivo* studies revealed that both ^{18}F-labeled metallopeptides possessed good tumor uptake in B16F10 murine model with high MC1R expression, while much lower uptake in A375M human melanoma xenografts. Moreover, **^{18}F-FP-RMSH-1** displayed more favorable *in vivo* performance in terms of higher tumor uptake and much lower accumulation in kidney and liver, when compared to **^{18}F-FP-RMSH-2** at 2 h post-injection (p.i.). **^{18}F-FP-RMSH-1** also displayed lower liver and lung uptake when compared with the same peptide labeled with ^{18}F-SFB (named as **^{18}F-FB-RMSH-1**). Small animal PET imaging of **^{18}F-FP-RMSH-1** in mice bearing B16F10 tumors at 1 and 2 h showed good tumor imaging quality. As expected, much lower tumor uptake and poorer tumor/normal organs contrast were observed for A375M model than that of B16F10 model. **^{18}F-FP-RMSH-1** also exhibited higher tumor uptake and better tumor retention when compared with **^{18}F-FB-RMSH-1**.

Conclusion—^{18}F-FP-RMSH-1 demonstrates significant advantages over **^{18}F-FB-RMSH-1** and **^{18}F-FP-RMSH-2**. It is a promising PET probe for imaging MC1R positive melanoma and MC1R expression *in vivo*.

Keywords

α-MSH; MC1R; PET; Malignant Melanoma; Metallopeptide, ^{18}F

*Author to whom correspondence should be addressed: Zhen Cheng, Ph.D, Molecular Imaging Program at Stanford, Department of Radiology and Bio-X Program, Canary Center at Stanford for Cancer Early Detection, 1201 Welch Road, Lucas Expansion, P095, Stanford University, Stanford, CA 94305-5484, 650-723-7866 (V), 650-736-7925(Fax), zcheng@stanford.edu .

INTRODUCTION

The incidence of malignant melanoma in western countries keeps increasing in the last two decades. According to the National Cancer Institute, there will be an estimated 68,000 new cases and 8,650 deaths in the United States in 2010. Although melanoma represents only 5% of all skin cancer subtypes, it contributes to more than 50% of deaths related to skin cancer (1,2). Melanoma is an aggressive disease with high metastatic potential and resistance to cytotoxic agents. Currently, early diagnosis and accurate staging of melanoma remain crucial for improvement of management of melanoma patients (3,4).

Melanocortin type 1 receptor (MC1R) is a G-protein coupled receptor and has been found to be over-expressed in many types of murine and human melanomas, making it an attractive target for receptor based melanoma imaging and therapy (5,6). Over the last two decades, a wide variety of alpha-melanocyte-stimulating hormone (α-MSH) peptides have been developed and extensively studied for MC1R targeted melanoma imaging and treatment (7,8). To date, two classes of α-MSH analogs have shown the most promising results for *in vivo* targeting of MC1R positive melanoma. One class is the linear α-MSH, Ac-Nle-Asp-His-d,Phe-Arg-Trp-Gly-Lys-NH_2 (referred to as NAPamide) and its analogs (9-12); the other is transition metal rhenium cyclized α-MSH, ReO[$Cys^{3,4,10}$, d,Phe^{7}, Arg^{11}]α-$MSH_{3–13}$ [referred to as ReCCMSH(Arg^{11})], based metallopeptides (13-18).

In our previous research, both NAPamide and ReCCMSH(Arg^{11}) analogs had been synthesized and radiolabeled with a well-established radiofluorination synthon, *N*-succinimidyl-4-^{18}F-fluorobenzoate (^{18}F-SFB) for positron emission tomography (PET) imaging of melanoma (12,19). The resulting ^{18}F-probes exhibited good tumor imaging contrast as early as 1 h post-injection (p.i.) in B16F10 tumor mouse models. Compared with ^{18}F-SFB labeled NAPamide, ^{18}F-SFB conjugated ReCCMSH(Arg^{11}) peptides displayed higher tumor uptake and retention, suggesting the advantages of rhenium cyclized CCMSH(Arg^{11}) as a scaffold for developing MC1R PET imaging agents (19). Overall, these pioneer studies highlight that ^{18}F-SFB labeled α-MSH peptides can efficiently target malignant melanoma with overexpression of MC1R in mice and they can be promising candidates for MC1R targeted melanoma PET imaging.

However, ^{18}F-SFB conjugated ReCCMSH (Arg^{11}) peptides also show moderate liver and lung uptake and relatively high uptake in gallbladder, which is unfavorable for clinical translation (19). In this research, we aimed to further optimize the *in vivo* behavior of ^{18}F labeled α-MSH metallopeptides for melanoma PET imaging. 4-nitrophenyl-2-[^{18}F]fluoropropionate (^{18}F-NFP) is a small prosthetic group with less hydrophobicity and has been widely used for radiofluorination of many peptides (20). The ^{18}F-NFP conjugated galacto-RGD peptide has even been evaluated in patients of different solid tumors for tumor angiogenesis imaging (21-23). The promising results suggested NFP as an attractive labeling moiety. Herein, we report the radiosynthesis of ^{18}F-NFP labeled Ac-d,Lys-ReCCMSH(Arg^{11}) peptides (two isomers, abbreviated as **RMSH-1** and **RMSH-2**, respectively) (Figure 1). The resulting probes **^{18}F-FP-RMSH-1** and **^{18}F-FP-RMSH-2** were then evaluated in C57BL/6 mice bearing subcutaneous murine B16F10 melanoma tumors with high levels of the MC1R and Foxn1 nude mice bearing human A375M melanoma with low levels of the MC1R.

MATERIALS AND METHODS

General

^{125}I-(Tyr^2)-[Nle^4,D-Phe^7]-α-MSH [^{125}I-(Tyr^2)-NDP] was purchased from Perkin Elmer (Waltham, MA). All N-α-Fmoc-protected amino acids were purchased from Advanced Chemtech (Louisville, KY). Dimethylformamide (DMF) and methylene chloride were from Fisher Scientific (Fair Lawn, NJ). Piperidine (20%) in DMF and 0.4 M of N-methylmorpholine in DMF were from Protein Technologies Inc. (Tucson, AZ). Trifluoroacetic acid (TFA), O-benzotriazole-*N*,*N*,*N*',*N*'-tetramethyluronium hexafluoro-phosphate (HBTU), and 4-(2′,4′-dimethoxyphenyl-Fmoc-aminomethyl)-phenoxy resin (Rink amide resin LS, 100-200 mesh, 1% DVB, 0.2 mmol/g) were from Advanced Chemtech. Pyridine, acetic anhydride, acetic acid, and anhydrous ether were from J.T.Baker (Phillipsburg, NJ). Triisopropylsilane (TIPS), N,N'-Diisopropylethylamine (DIPEA) and 1, 2-ethanedithiol (EDT) were purchased from Sigma-Aldrich (Milwaukee, WI). High performance liquid chromatography (HPLC) grade acetonitrile (CH_3CN) and Millipore 18 mΩ water were used for peptide purifications. 4-nitrophenyl 2-fluoropropionate (^{19}F-NFP) was synthesized as previously reported (24). All other standard synthesis reagents were purchased from Sigma-Aldrich Chemical Co. (St. Louis, MO). All the other general materials (cell lines, mice, etc.) and instruments [reverse phase HPLC, radioactive dose calibrator, and electrospray ionization mass spectrometry (ESI-MS) or matrix-assisted laser desorption/ionization time of flight mass spectrometry (MALDI-TOF-MS)] are the same as previously reported (12). A375M cell line was a generous gift from Dr. M. Kolodny; University of California, Los Angeles, CA, and B16/F10 murine melanoma cells were obtained from the American Type Tissue Culture Collection (Manassas, VA). C57BL/6 and Fox Chase SCID mice were purchased from Charles River Laboratories (Boston, MA).

Synthesis of RMSH and ^{19}F-FP-RMSH

The rhenium cyclized metallopeptide, RMSH, was synthesized as previously reported using the Ac-d,Lys-CCMSH(Arg^{11}) peptide (amino acid sequence: Ac-kCCEHdFRWCRPV-NH_2) and rhenium-glucoheptonate transchelation reaction (19). Two major products (isomers **RMSH-1** and **RMSH-2**) with identical molecular weight (MW) but different HPLC retention times were obtained. The reference standard **^{19}F-FP-RMSH-1** and **2** were then prepared by reaction of the metallopeptides with ^{19}F-NFP (24). Briefly, **RMSH-1** or **2** (1 μmol) in DMSO (100 μL) was added to ^{19}F-NFP (5 μmol) in DMSO (100 μL), followed by addition of DIPEA (5 μL). The mixture was heated at 60 °C for 2 h. After it cooled down to room temperature, the reaction solution was quenched by adding TFA (50 μL) and injected into a semi-preparative HPLC for purification. The flow rate was 3 mL/minute, with the mobile phase starting at 95% solvent A and 5% solvent B (0-3 minutes), going to 35% solvent A and 65% solvent B at 33 minutes, then going to 15% solvent A and 85 % solvent B and maintaining this solvent composition for another 3 minutes (36-39 minutes), and returning to initial solvent composition after 42 minutes had elapsed. Fractions containing the product were collected, lyophilized and characterized by ESI-MS or MALDI-TOF-MS.

Radiosynthesis of ^{18}F-FP-RMSH-1 and 2

The radiofluorination synthon, ^{18}F-NFP was prepared based on the procedure reported previously (23,25). ^{18}F-NFP (specific activity of 0.4-1.0 Ci/μmol or 14.7-37 GBq/μmol) dissolved in acetonitrile (100 μL) was then added to the peptide (**RMSH-1** or **2**; 100 μg) dissolved in DMSO and reacted for 20 min at 60 °C. After adding TFA (50 μL) to quench the reaction, the reaction solution was injected into a semipreparative HPLC using the same elution gradient as the one used in the synthesis of cold **^{19}F-FP-RMSH (1** or **2)**. The HPLC fractions containing the radiolabeled product were subsequently collected, combined and evaporated with a rotary evaporator to dryness. The radiolabeled peptide was reconstituted

in phosphate-buffered saline (PBS, 0.01 M, pH 7.4) and passed through a 0.22 μm Millipore filter into a sterile vial for *in vitro* and animal experiments.

In Vitro Cell Binding Assay

B16F10 murine melanoma cells were cultured in the Dulbecco's Modified Eagle High-Glucose Medium (DMEM) supplemented with 10% fetal bovine serum (FBS) and penicillin and streptomycin. The cells were maintained in 37 °C, 5% CO_2 humidified incubator. The receptor binding affinity studies of **^{19}F-FP-RMSH-1** and **2** for the MC1R were performed using B16F10 cells. Briefly, 0.5×10^6 cells were re-suspended in Dulbecco's Modified Eagle's Medium containing 25 mM HEPES, 0.2% BSA, and 0.3 mM 1,10-phenanthroline. The cells were then incubated at 37 °C for 90 minutes with either **^{19}F-FP-RMSH-1** or **2** (peptide concentration varying from 10^{-12}-10^{-6} M) and approximately 40,000 counts per minute (cpm) of ^{125}I-(Tyr^2)-NDP. Cells were washed three times with ice-cold PBS and the radioactivity of the cells was measured. Data was analyzed by Graphpad Prism 5.0 (Northampton, MA). The IC_{50} values, the concentration of competitor required to inhibit 50% of the radioligand binding, of the peptides were calculated.

Biodistribution Studies

All animal experiments were performed in compliance with a protocol approved by Stanford University Institutional Animal Care and Use Committee. Five to six-week old male C57BL/6 mice were implanted with 1×10^6 B16F10 murine melanoma cells and Foxn1 nude mice were inoculated with 3×10^6 A375M human melanoma cells in the right flank. When the diameters of the tumors reached around 8 mm, approximately 110-130 μCi (4.07-4.81 MBq) of **^{18}F-FP-RMSH-1** or **2** was injected into each mouse through tail vein. After injection of the radiotracer, the B16F10 mice (n=3) were sacrificed at 1, 2 and 4 h p.i., while A375M (n=3) mice were sacrificed at 2 h p.i. by carbon dioxide. Tumors, blood and major organs of interest were harvested, weighed, and counted in a Wallac 1480 automated γ-counter (Perkin Elmer, Waltham, MA). The radioactivity uptake in tumors and normal tissues was expressed as a percentage of the injected radioactive dose per gram of tissue (% ID/g).

Small-Animal PET Imaging Studies

PET imaging of tumor-bearing mice was performed on a small-animal PET R4 rodent model scanner (Siemens Medical Solutions USA, Inc., Knoxville, TN). The mice bearing B16F10 or A375M tumors were injected with 110-130 μCi (4.07-4.81 MBq) of **^{18}F-FP-RMSH-1** or **2** through tail vein. At 1 and 2 h p.i., the mice were anesthetized with 2% isofluorane, and placed in the prone position near the central field of view in the small-animal PET. Five-minute static scans were obtained and images were reconstructed by a two-dimensional ordered subsets expectation maximum (OSEM) algorithm. Regions of interest (ROIs) were then drawn over the tumor or organ of interest on decay-corrected whole-body coronal images. The mean counts per pixel per minute were obtained from the ROI and converted to counts per milliliter per minute by using a calibration constant. By assuming a tissue density of 1 g/mL, the ROIs were converted to counts·g^{-1}·minute^{-1}. An image ROI-derived %ID/g of tissue was then determined by dividing counts per gram per minute with injected dose (ID). No attenuation correction was performed.

Statistical Methods

Statistical analysis was performed using the Student's *t*-test for unpaired data. A 95% confidence level was chosen to determine the significance between groups, with $P < 0.05$ being significantly different.

RESULTS

Chemistry, Radiochemistry and IC_{50}

The linear peptide, Ac-d,Lys-CCMSH(Arg^{11}), could react with the rhenium-glucoheptonate to produce two major products (**RMSH-1** and **RMSH-2**) with same molecular weight (MW) and similar binding affinities to MC1R, which was reported previously (19). The non-radioactive fluorinated metallopeptides were then prepared by conjugation with cold ^{19}F-NFP to allow for characterization of the ^{18}F labeled counterparts. Under the HPLC gradient (5-65% over 30 minutes) used in the study, the retention times for **^{19}F-FP-RMSH-1** and **2** were found to be 16.6 minutes and 18.1 minutes, respectively (Figure 2). The desired products were purified by semi-preparative HPLC (>90% yield and >95% purity) and characterized by MALDI-TOF-MS. For all the metallopeptides prepared above, the measured MW was consistent with the expected MW: *m/z* = 1878.1 for $[M+H]^+$ ($C_{73}H_{104}FN_{23}O_{17}ReS_3$, Calculated MW = 1878.2). Receptor binding assay showed that the IC of ^{19}50**F-FP-RMSH-1** and **2** were 6.1 and 33.7 nM, respectively (Table 1).

Similarly, **^{18}F-FP-RMSH-1** and **2** were prepared by conjugation of **RMSH-1** or **2** with the radioactive 18F-NFP. Based on the retention times acquired from the nonradioactive fluorinated peptides, the radiofluorinated products were identified and collected using the same HPLC gradient. The total radiosynthesis time for making the radiopeptide took about 100 minutes. The decay-corrected radiochemical yields of **^{18}F-FP-RMSH-1** and **2** were based on ^{18}F-NFP were 12.0% ± 2.7% and 10.5% ± 1.8% (n = 4) at the end of synthesis (EOS). The radiochemical purities of the labeled peptides were over 95%, as verified by analytical radio-HPLC. Since the difference in retention times of radiolabeled and unlabeled peptide was greater than 1.5 minutes, the radiofluorinated **RMSH-1** and **2** were easily separated from their non-radiolabeled counterparts by HPLC. The specific activity of the two **^{18}F-FP-RMSH-1** and **2** were estimated to be ~20 GBq/μmol (decay corrected) on the basis of the labeling agent ^{18}F-NFP.

In Vivo Biodistribution of ^{18}F-FP-RMSH-1 and 2

The *in vivo* biodistribution studies of both **^{18}F-FP-RMSH-1** and **2** were examined in B16F10 murine allograft and A375M human xenograft melanoma-bearing mice. As shown in Table 2, for **^{18}F-FP-RMSH-1**, the uptake in B16F10 tumor with high expression of MC1R was 1.80 ± 0.18, 2.12 ± 1.08, and 1.09 ± 0.23 %ID/g at 1, 2 and 4 h p.i., suggesting good tumor uptake and retention of this PET probe. **^{18}F-FP-RMSH-1** also displayed rapid blood clearance and low uptake in muscle, resulting in decent tumor/blood and tumor/muscle ratios (3.80 ± 0.89 and 9.36 ± 3.98, respectively) at 2 h p.i. It was also noted that **^{18}F-FP-RMSH-1** displayed much lower uptake in lung and liver (0.80 ± 0.03 and 0.78 ± 0.05, respectively) compared with **^{18}F-FB-RMSH-1** (19). Also compared with **^{18}F-FB-RMSH-1, ^{18}F-FP-RMSH-1** showed lower kidney uptake in B16F10 tumor bearing mice ($P < 0.05$). The level of accumulation in kidney was 8.82 ± 0.76 and 6.76 ± 0.82 %ID/g at 1 h and 2 h p.i. respectively for **^{18}F-FP-RMSH-1**. For the A375M model, tumor uptake of **^{18}F-FP-RMSH-1** was only 0.84 ± 0.39 %ID/g at 2 h p.i., which was significantly lower than in B16F10 tumors ($P < 0.01$).

For **^{18}F-FP-RMSH-2**, the uptake in B16F10 tumor model was 0.78 ± 0.10 %ID/g at 2 h p.i., which was much lower than that of **^{18}F-FP-RMSH-1** ($P < 0.05$). Meanwhile, **^{18}F-FP-RMSH-2** showed much higher kidney uptake of 15.13 ± 0.88 %ID/g at 2 h p.i. ($P < 0.05$). In addition, **^{18}F-FP-RMSH-2** demonstrated higher uptake in liver when compared to **^{18}F-FP-RMSH-1**. For other major organs including lung, spleen, pancreas and stomach, **^{18}F-FP-RMSH-2** exhibited similar uptake as that of **^{18}F-FP-RMSH-1** ($P > 0.05$). Lastly, **^{18}F-**

FP-RMSH-2 revealed very low tumor uptake (0.63 ± 0.19 %ID/g) but high uptake (13.45 ± 0.91 %ID/g) was observed in kidneys at 2 h p.i in A375M tumor model.

Small-Animal PET Imaging

Small-animal PET imaging of mice bearing B16F10 using **^{18}F-FP-RMSH-1** and **2** was performed and the imaging results were compared (Figure 3A, B). Visual examination showed that **^{18}F-FP-RMSH-1** uptake in tumor was higher than that of **^{18}F-FP-RMSH-2** at both 1 and 2 h p.i. Both probes showed moderate to high uptake in liver and kidney. Further quantification analysis of small-animal PET images demonstrated that **^{18}F-FP-RMSH-2** had a much higher uptake in kidney than that of **^{18}F-FP-RMSH-1** ($P < 0.01$) at 1 and 2 h p.i. (Figure 4). Improved quality of PET images was also observed at 2 h p.i. for **^{18}F-FP-RMSH-1**. Based on the above findings, **^{18}F-FP-RMSH-1** was selected as a PET probe for further evaluation.

^{18}F-FP-RMSH-1 was then imaged in the nude mice bearing A375M melanoma with low MC1R expression at 1 and 2 h (Figure 3C). Compared with B16F10 tumor bearing mice, much lower tumor uptake and poor tumor-to-background ratio were observed in A375M tumors at both time points. A375M tumor was barely discernable while high activity accumulation in kidneys was still observed.

DISCUSSION

It has been reported that overexpression of MC1R may correlate with the prognosis of malignant melanoma (26,27). Peptide based radioactive probes have been extensively studied for tumor receptor targeted imaging and therapy (28-30). Recently a number of studies have also been performed to develop molecular probes that specifically target MC1R in melanoma (12,19). However, ^{18}F-SFB labeled **RMSH** has its own limitations such as suboptimal tumor uptakes and relatively high uptakes in liver and lung. Thus, the major goal of this research is to study whether we can further optimize the *in vivo* profile of ^{18}F-labeled **RMSH** analogs by using a different radiofluorination synthon, ^{18}F-NFP. The resulting PET probe, **^{18}F-FP-RMSH**, was also studied for its ability to image melanoma and differential MC1R expression in tumor mice models.

Two isomers of rhenium cyclized Ac-d,Lys-CCMSH(Arg^{11}), **RMSH-1** and **2** were reproducibly formed in previous studies and proved to possess high MC1R binding affinity in nanomolar (nM) range. Further modification of **RMSH** with the small prosthetic group ^{19}F-NFP only slightly reduced their affinities, as evidenced by *in vitro* cell binding assays (Table 1). The NFP conjugation to **RMSH** did not change the binding capability to B16F10 cells which overexpress MC1R. In addition, **^{19}F-FP-RMSH-1** displays much higher MC1R binding affinity than that of **^{19}F-FP-RMSH-2** (6.1 *vs.* 33.7 nM), which is in consistence with the study of the ^{19}F-SFB conjugated **RMSH** peptides (19). Since the affinities of both compounds are in the low nM and thus very encouraging, further *in vivo* evaluation of the ^{18}F-NFP labeled metallopeptides is warranted.

In biodistribution studies in B16F10 tumor mice model, a higher tumor uptake of **^{18}F-FP-RMSH-1** can be observed compared to **^{18}F-FP-RMSH-2** along with much lower kidney and liver uptake for **^{18}F-FP-RMSH-1** at 2 h ($P < 0.05$). The higher tumor uptake while lower kidney uptake was further evidenced by small-animal PET imaging as well as quantification analysis of PET images. For **^{18}F-FP-RMSH-1**, B16F10 tumors are clearly delineated over the background at 1 and 2 h p.i., while **^{18}F-FP-RMSH-2** shows much less prominent tumor uptake (Figure 3 A and B). The quantification analysis of small-animal PET images further reveals significant difference in tumor, liver and kidney uptake between the two probes ($P < 0.01$) (Figure 4). **^{18}F-FP-RMSH-2** exhibits a much lower tumor uptake

but higher kidney uptake than those of **^{18}F-FP-RMSH-1** at both 1 and 2 h in B16F10 tumor bearing mice. In A375M model, the tumor uptake is low for both **^{18}F-FP-RMSH-1** and **2**. Interestingly, the higher uptake in liver and kidney for **^{18}F-FP-RMSH-2** compared with **^{18}F-FP-RMSH-1** ($P < 0.05$) may further suggest the different clearance time of these two isomers**.** Overall, **^{18}F-FP-RMSH-1** clearly displays more favorable *in vivo* properties, which suggests that it could be a better candidate for imaging MC1R *in vivo*.

^{18}F-FP-RMSH-1 exhibits longer retention times in B16F10 tumor than all other normal organs but kidney (Table 2). The tumor to blood and tumor to muscle ratios reach the highest levels at 4 h. More importantly, it is noticed that **^{18}F-FP-RMSH-1** displays high tumor to background ratios, for example, tumor to blood and tumor to muscle ratios at 4 h are 7.45 ± 0.69 and 16.97 ± 1.73, respectively. While for another two radiofluorinated α-MSH peptides reported previously, **^{18}F-FB-NAPamide** and **^{18}F-FB-RMSH-1**, their tumor to blood ratio at 4 h are only 3.60 ± 0.37 and 1.65 ± 0.11, respectively; and their tumor to muscle ratio at 4 h are 7.46 ± 2.68 and 5.24 ± 1.43, respectively (12,19). These increased tumor to background ratios as well as tumor residence time would make longitudinal observation of the malignant melanoma with overexpression of MC1R more feasible when using NFP conjugated **RMSH-1** as PET probes. For the A375M tumor model, the tumors are barely noticeable and show background uptake at 1 and 2 h p.i., when the mice were injected with **^{18}F-FP-RMSH-1** (Figure 3C). This low uptake is likely caused by nonspecific uptake. The better PET imaging quality in B16F10 tumor compared to that in the A375M suggests that **^{18}F-FP-RMSH-1** could differentiate melanoma with different MC1R expression in living subjects.

More importantly, compared with previous ^{18}F-SFB conjugated **RMSH-1** (**^{18}F-FB-RMSH-1**) that possesses moderate lung and liver uptake in the B16F10 tumor model (19), **^{18}F-FP-RMSH-1** shows similar tumor uptake at 1 and 2 h but the uptake gets significantly higher than that of **^{18}F-FB-RMSH-1** at 4 h ($P < 0.05$). The background uptake, particularly in the liver and lung, is much lower for **^{18}F-FP-RMSH-1**. Much higher tumor-to-blood and tumor-to-muscle ratios are also observed for **^{18}F-FP-RMSH-1** than that of **^{18}F-FB-RMSH-1**. Furthermore, the liver and lung uptake are lower for **^{18}F-FP-RMSH-2** when compared with **^{18}F-FB-RMSH-2** in both models ($P < 0.05$). All these observations highlight that different radiofluorination methods have significant impact in this metallopeptide's *in vivo* properties. Additionally, these observations further suggest that the uptake in liver and lung are due to nonspecific accumulation.

Taken together, ^{18}F-NFP shows advantages over ^{18}F-SFB for labeling of **RMSH** peptides. Compared to **^{18}F-FB-RMSH-1**, **^{18}F-FP-RMSH-1** is more promising for translation into melanoma MC1R PET imaging in clinic. The relatively low liver and lung uptake of **^{18}F-FP-RMSH-1** also validate the possibility of using it as a potential PET probe for early detection of malignant melanoma metastasis in these regions. **^{18}F-FP-RMSH-1** seems by far the best radiofluorinated probe reported for imaging MC1R expression *in vivo*.

CONCLUSION

In summary, radiofluorinated rhenium cyclized α-MSH analog, **^{18}F-FP-RMSH-1** and **2** were successfully synthesized. Their characteristics including binding affinities and *in vivo* profiles were investigated in this study. The **^{18}F-FP-RMSH-1** demonstrates significant advantages over **^{18}F-FB-RMSH-1** and **^{18}F-FP-RMSH-2**. **^{18}F-FP-RMSH-1** displays favorable *in vivo* pharmacokinetics in MC1R over-expressing tumor mice models. It is a promising PET probe for imaging MC1R positive melanoma and MC1R expression *in vivo*.

Acknowledgments

This work was supported, in part, by National Cancer Institute (NCI) *In Vivo* Cellular Molecular Imaging Center (ICMIC) grant P50 CA114747 and Melanoma Research Alliance. We also thank the Radiochemistry Facility at Stanford for ^{18}F production, and Dr. Zhe Liu for his help on peptides synthesis.

Abbreviations

α-MSH	alpha-melanocyte stimulating hormone
MC1R	melanocortin type 1 receptor
PET	positron emission tomography
SPECT	single photon emission spectroscopy
HPLC	high-performance liquid chromatography
^{18}F-NFP	4-nitrophenyl 2-^{18}F-fluoropropionate
^{18}F-SFB	*N*-succinimidyl-4-^{18}F-fluorobenzoate
[^{18}F]FDG	2-deoxy-2-[^{18}F]fluoro-D-glucose
p.i.	postinjection

REFERENCES

(1). Gray-Schopfer V, Wellbrock C, Marais R. Melanoma biology and new targeted therapy. Nature. 2007; 445:851–7. [PubMed: 17314971]

(2). Jemal A, Siegel R, Xu J, Ward E. Cancer statistics. CA Cancer J Clin. 2010; 60:277–300. [PubMed: 20610543]

(3). Rohren EM, Turkington TG, Coleman RE. Clinical applications of PET in oncology. Radiology. 2004; 231:305–32. [PubMed: 15044750]

(4). Belhocine TZ, Scott AM, Even-Sapir E, Urbain JL, Essner R. Role of nuclear medicine in the management of cutaneous malignant melanoma. J Nucl Med. 2006; 47:957–67. [PubMed: 16741305]

(5). Siegrist W, Solca F, Stutz S, Giuffre L, Carrel S, Girard J, Eberle AN. Characterization of receptors for alpha-melanocyte-stimulating hormone on human melanoma cells. Cancer Res. 1989; 49:6352–8. [PubMed: 2804981]

(6). Siegrist W, Stutz S, Eberle AN. Homologous and heterologous regulation of alpha-melanocyte-stimulating hormone receptors in human and mouse melanoma cell lines. Cancer Res. 1994; 54:2604–10. [PubMed: 8168086]

(7). Ren G, Pan Y, Cheng Z. Molecular probes for malignant melanoma imaging. Curr Pharm Biotechnol. 2010; 11:590–602. [PubMed: 20497118]

(8). Miao Y, Quinn T. Peptide-targeted radionuclide therapy for melanoma. Crit Rev Oncol Hematol. 2008; 67:213–28. [PubMed: 18387816]

(9). Froidevaux S, Calame-Christe M, Tanner H, Eberle AN. Melanoma targeting with DOTA-alpha-melanocyte-stimulating hormone analogs: structural parameters affecting tumor uptake and kidney uptake. J Nucl Med. 2005; 46:887–95. [PubMed: 15872364]

(10). Froidevaux S, Calame-Christe M, Tanner H, Sumanovski L, Eberle AN. A novel DOTA-alpha-melanocyte-stimulating hormone analog for metastatic melanoma diagnosis. J Nucl Med. 2002; 43:1699–706. [PubMed: 12468522]

(11). Cheng Z, Xiong Z, Subbarayan M, Chen X, Gambhir SS. ^{64}Cu-labeled alpha-melanocyte-stimulating hormone analog for microPET imaging of melanocortin 1 receptor expression. Bioconjug Chem. 2007; 18:765–72. [PubMed: 17348700]

(12). Cheng Z, Zhang L, Graves E, Xiong Z, Dandekar M, Chen X, Gambhir SS. Small-animal PET of melanocortin 1 receptor expression using a ^{18}F-labeled alpha-melanocyte-stimulating hormone analog. J Nucl Med. 2007; 48:987–94. [PubMed: 17504880]

(13). Chen J, Cheng Z, Hoffman TJ, Jurisson SS, Quinn TP. Melanoma-targeting properties of ^{99m}technetium-labeled cyclic alpha-melanocyte-stimulating hormone peptide analogues. Cancer Res. 2000; 60:5649–58. [PubMed: 11059756]

(14). Chen J, Cheng Z, Owen NK, Hoffman TJ, Miao Y, Jurisson SS, Quinn TP. Evaluation of an ^{111}In-DOTA-rhenium cyclized alpha-MSH analog: a novel cyclic-peptide analog with improved tumor-targeting properties. J Nucl Med. 2001; 42:1847–55. [PubMed: 11752084]

(15). Cheng Z, Chen J, Miao Y, Owen NK, Quinn TP, Jurisson SS. Modification of the structure of a metallopeptide: synthesis and biological evaluation of ^{111}In-labeled DOTA-conjugated rhenium-cyclized alpha-MSH analogues. J Med Chem. 2002; 45:3048–56. [PubMed: 12086490]

(16). Cheng Z, Chen J, Quinn TP, Jurisson SS. Radioiodination of rhenium cyclized alpha-melanocyte-stimulating hormone resulting in enhanced radioactivity localization and retention in melanoma. Cancer Res. 2004; 64:1411–8. [PubMed: 14973076]

(17). McQuade P, Miao Y, Yoo J, Quinn TP, Welch MJ, Lewis JS. Imaging of melanoma using ^{64}Cu- and ^{86}Y-DOTA-ReCCMSH(Arg^{11}), a cyclized peptide analogue of alpha-MSH. J Med Chem. 2005; 48:2985–92. [PubMed: 15828837]

(18). Giblin MF, Wang N, Hoffman TJ, Jurisson SS, Quinn TP. Design and characterization of alpha-melanotropin peptide analogs cyclized through rhenium and technetium metal coordination. Proc Natl Acad Sci U S A. 1998; 95:12814–8. [PubMed: 9788997]

(19). Ren G, Liu Z, Miao Z, Liu H, Subbarayan M, Chin FT, Zhang L, Gambhir SS, Cheng Z. PET of malignant melanoma using ^{18}F-labeled metallopeptides. J Nucl Med. 2009; 50:1865–72. [PubMed: 19837749]

(20). Liu S, Shen B, Chin F, Cheng Z. Recent Progress in Radiofluorination of Peptides for PET Molecular Imaging. Curr. Org. Synth. 2010; 7 In Press.

(21). Guhlke S, Coenen HH, Stöcklin G. Fluoroacylation agents based on small n.c.a. ^{18}F-fluorocarboxylic acids. Applied Radiation and Isotopes. 1994; 45:715–727.

(22). Haubner R, Kuhnast B, Mang C, Weber WA, Kessler H, Wester HJ, Schwaiger M. ^{18}F-Galacto-RGD: synthesis, radiolabeling, metabolic stability, and radiation dose estimates. Bioconjug Chem. 2004; 15:61–9. [PubMed: 14733584]

(23). Beer AJ, Haubner R, Sarbia M, Goebel M, Luderschmidt S, Grosu AL, Schnell O, Niemeyer M, Kessler H, Wester HJ, Weber WA, Schwaiger M. Positron emission tomography using ^{18}F-Galacto-RGD identifies the level of integrin alpha(v)beta3 expression in man. Clin Cancer Res. 2006; 12:3942–9. [PubMed: 16818691]

(24). Liu S, Liu Z, Chen K, Yan Y, Watzlowik P, Wester HJ, Chin FT, Chen X. ^{18}F-Labeled Galacto and PEGylated RGD Dimers for PET Imaging of alpha(v)beta (3) Integrin Expression. Mol Imaging Biol. 2009

(25). Haubner R, Kuhnast B, Mang C, Weber WA, Kessler H, Wester HJ, Schwaiger M. ^{18}F-Galacto-RGD: synthesis, radiolabeling, metabolic stability, and radiation dose estimates. Bioconjugate Chemistry. 2004; 15:61–9. [PubMed: 14733584]

(26). Benjamin CL, Melnikova VO, Ananthaswamy HN. Models and mechanisms in malignant melanoma. Mol Carcinog. 2007; 46:671–8. [PubMed: 17570501]

(27). Bohm M, Luger TA, Tobin DJ, Garcia-Borron JC. Melanocortin receptor ligands: new horizons for skin biology and clinical dermatology. J Invest Dermatol. 2006; 126:1966–75. [PubMed: 16912693]

(28). Liu S. Radiolabeled cyclic RGD peptides as integrin alpha(v)beta(3)-targeted radiotracers: maximizing binding affinity via bivalency. Bioconjug Chem. 2009; 20:2199–213. [PubMed: 19719118]

(29). Lee S, Xie J, Chen X. Peptides and peptide hormones for molecular imaging and disease diagnosis. Chem Rev. 2010; 110:3087–111. [PubMed: 20225899]

(30). Lewis JS, Anderson CJ. Radiometal-labeled somatostatin analogs for applications in cancer imaging and therapy. Methods Mol Biol. 2007; 386:227–40. [PubMed: 18604948]

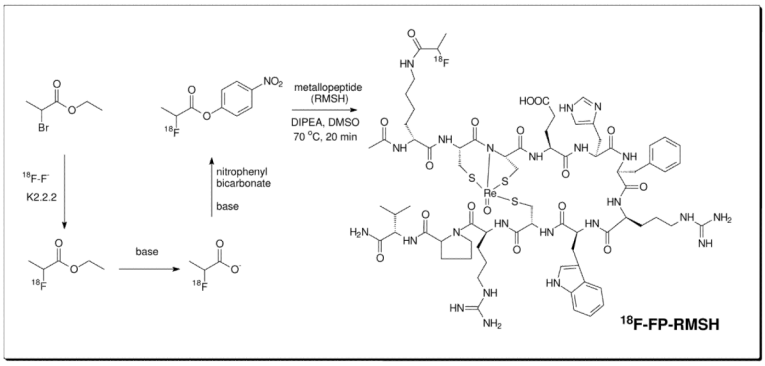

Figure 1.
Scheme of radiosynthesis of **^{18}F-FP-RMSH**

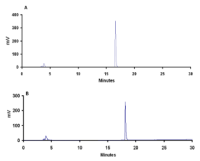

Figure 2.
HPLC profiles of **^{19}F-FP-RMSH-1** (A) and**2** (B).

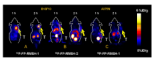

Figure 3.
Representative decay-corrected coronal small-animal PET images of mice bearing B16F10 tumors on right shoulder at 1 and 2 h after tail vein injection of **^{18}F-FP-RMSH-1** (A) and **2** (B) (n=3 for each group). T stands for tumor. (**C**) Representative decay-corrected coronal small-animal PET images of A375M tumor bearing mice at indicated time points after tail vein injection of **^{18}F-FP-RMSH-1**.

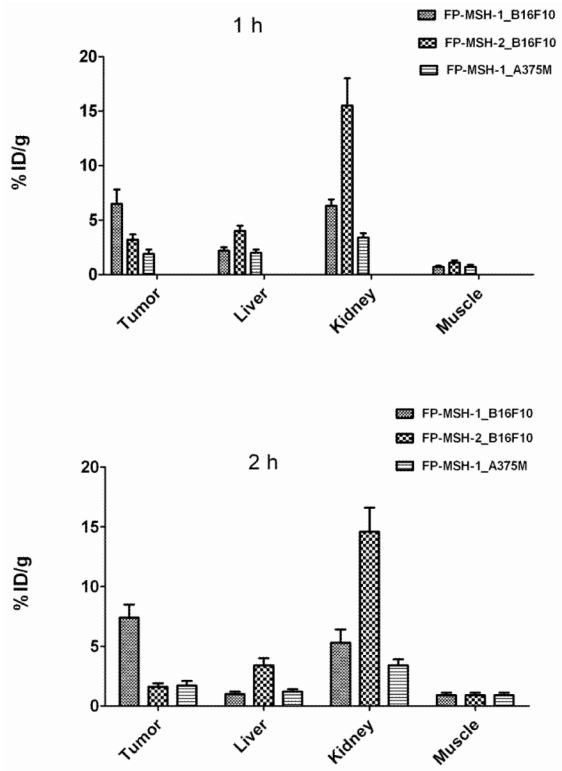

Figure 4.

PET quantification of tumor and other major organs uptake derived from 1 (**A**) and 2 h (**B**) after tail vein injection of **^{18}F-FP-RMSH-1** or **2**. Data are shown as mean ±SD %ID/g (n = 3).

Table 1

IC_{50} values of the fluorinated α-MSH analogues and their expected and measured molecular weight (M.W.) for $[M+H]^+$ by ESI-MS or MALDI-TOF-MS

Peptides	Expected M.W.	Measured M.W.	IC_{50} (nM)
^{19}F-FP-RMSH-1	1878.2	1878.1	6.1 ± 0.6
^{19}F-FP-RMSH-2	1878.2	1878.1	33.7 ± 3.0

Bioconjug Chem. Author manuscript; available in PMC 2011 December 15.

Table 2

Biodistribution data for **^{18}F-FP-MSH-1** and **2** in C57BL/6 mice bearing subcutaneously xenotransplanted B16F10 murine melanoma and Foxn1 nude mice bearing A375M human melanoma. Data were expressed as mean ± SD, indicating the percentage administered activity (injected dose) per gram of tissue (%ID/g) after intravenous injection of 110- 130 μCi (4.01-4.87 MBq) tracers (n = 3)

Organ (%ID/g)	^{18}F-FP-RMSH-1				^{18}F-FP-RMSH-2	
	B16F10			A 375M	B16F10	A 375M
	1h	2h	4h	2h	2h	2h
Tumor	1.80 ± 0.18	2.12 ± 1.08	1.09 ± 0.23	*0.84 ± 0.39	*0.78 ±0.10	*0.63 ± 0.19
Blood	0.90 ± 0.10	0.42 ± 0.06	0.15 ± 0.04	0.33 ± 0.22	0.31 ± 0.11	0.20 ± 0.09
Heart	0.55 ± 0.03	0.31 ± 0.06	0.14 ± 0.06	0.41 ± 0.19	0.21 ± 0.06	0.18 ± 0.07
Liver	1.36 ± 0.22	0.78 ± 0.05	0.44 ± 0.11	0.69 ± 0.21	*1.97 ± 0.17	1.66 ± 0.08
Lung	1.72 ± 0.16	0.80 ± 0.03	0.31 ± 0.07	0.68 ± 0.10	0.64 ± 0.15	0.47 ± 0.21
Muscle	0.33 ± 0.11	0.17 ± 0.03	0.06 ± 0.01	0.19 ± 0.08	0.20 ± 0.05	0.10 ± 0.02
Spleen	0.61 ± 0.05	0.34 ± 0.07	0.20 ± 0.04	0.34 ± 0.19	0.53 ± 0.03	0.27 ± 0.03
Brain	0.11 ± 0.04	0.11 ± 0.04	0.04 ± 0.01	0.05 ± 0.01	0.04 ± 0.01	0.04 ± 0.01
Intestine	0.99 ± 0.45	1.14 ± 0.80	0.29 ± 0.18	0.40 ± 0.19	0.91 ± 0.33	0.17 ± 0.00
Stomach	0.67 ± 0.31	0.47 ± 0.24	0.31 ± 0.07	0.44 ± 0.02	0.42 ± 0.14	0.52 ± 0.50
Pancreas	0.32 ± 0.08	0.18 ± 0.03	0.06 ± 0.01	0.78 ± 0.49	0.10 ± 0.03	0.09 ± 0.01
Bone	0.69 ± 0.18	0.68 ± 0.37	0.17 ± 0.09	0.23 ± 0.11	0.52 ± 0.08	0.25 ± 0.12
Kidney	8.82 ± 0.76	6.76 ± 0.82	4.41 ± 0.78	6.59 ± 1.53	*15.13 ± 0.88	*13.45 ± 0.91
Uptake Ratio						
Tumor / Blood	2.03 ± 0.33	3.80 ± 0.89	7.45 ± 0.69	3.11 ± 1.30	2.74 ± 0.80	2.90 ± 0.04
Tumor / Muscle	5.78 ± 1.35	9.36 ± 3.98	16.97 ± 1.73	4.49 ± 0.17	3.98 ± 1.09	6.40 ± 2.66

*P <0.05 when compared with ^{18}F-FP-RMSH-1 at 2h